

# Adhesion induced non-planar and asynchronous flow of a giant vesicle membrane in an external shear flow

Cyrille Vézzy,<sup>a</sup> Gladys Massiera<sup>b</sup> and Annie Viallat<sup>\*a</sup>

Received 15th January 2007, Accepted 19th March 2007

First published as an Advance Article on the web 3rd April 2007

DOI: 10.1039/b700550d

We show the existence of a flow at the surface of strongly adhering giant lipid vesicles submitted to an external shear flow. The surface flow is divided into two symmetric quadrants and presents two stagnation points (SP) on each side of the vesicle meridian plane. The position of these stagnation points depends strongly on the adhesion strength, characterized by the ratio of the contact zone diameter to the vesicle diameter. Contrary to the case of non-adhesive vesicles, streamlines do not lie in the shear plane. By avoiding the motionless contact zone, streamlines result in three-dimensional paths, strongly asymmetric away from the SP. Additional shearing dissipation may occur on the membrane surface as we observed that the mean rotational velocity of the membrane increases towards the vesicle SP, and is mainly determined by the adhesion induced vesicle shape.

## Introduction

Situations where soft deformable objects with a fluid interface like drops, vesicles and cells are subjected to hydrodynamic flows at low Reynolds numbers are involved in an increasing number of engineering and biophysical processes including microfluidics and emulsion processing,<sup>1</sup> biomechanics<sup>2</sup> and blood circulation.<sup>3,4</sup> Numerous studies have brought insights into the specificity of the motion of this class of particles under simple Poiseuille or shear flows.

In particular, it is well known that under simple shear flow, the fluidity of the particle interface allows surface flows, which are at the origin of a typical motion called tanktreading. This regime of motion, observed under suitable conditions of viscosity, aspect ratio of the particle and shear rate,<sup>5–7</sup> is characterized by a stationary particle shape, a steady finite inclination angle with respect to the flow direction and the rotation of the surface layer or of the membrane of the particle about its centre of mass.

The surface flow of the incompressible membrane of tanktreading red blood cells has long been observed from the position of small latex beads stuck onto the rotating membrane.<sup>4</sup> Similarly, the motion of lipid vesicle membranes has been reported for tanktreading vesicles in shear flow,<sup>8,9</sup> and for vesicles sliding along an inclined plane in a quiescent fluid,<sup>10</sup> by tracking small lipid defects linked to the membrane. It was observed both for red blood cells (biconcave disks) and spherical or ellipsoidal vesicles that all elements of the membrane flow on closed surface streamlines, which describe quasi-planar orbits in the shear plane.<sup>4,10</sup> The surface flow of

the red blood cell membrane, which is bound to a solid elastic cytoskeleton, is synchronous in the sense that the cyclic motions along the streamlines have one common frequency, the tanktreading frequency.<sup>4</sup> It means that adjacent membrane elements remain adjacent after a full revolution along the streamlines. The revolution velocity on the streamlines of vesicle surfaces has not been experimentally explored in detail. A short report on a non-spherical vesicle fixed by a thin lipid tube to the substrate, suggests that the angular velocity along the surface streamlines of the viscous membrane depends on the lateral streamline position with respect to the meridian orbit of the vesicle.<sup>11</sup>

The theoretical problem of the surface flow of a tanktreading fluid membrane with fixed area and bending rigidity in shear flow is complex. Using a simple surface velocity field and under the hypothesis of a synchronous motion along planar elliptical orbits, Keller and Skalak<sup>12</sup> analytically derived the equation of motion of a fluid ellipsoid and computed the tanktreading velocity. Secomb and Skalak<sup>13</sup> generated more realistic area-conserving velocity fields on the surface of ellipsoids. In this case, they showed that the motion along streamlines, which presented a curvature towards each end of the cell, resulted in less dissipation than the motion with planar orbits. More recently, Kraus *et al.*<sup>14</sup> proposed a numerical approach to deal with an incompressible membrane with bending rigidity and an ellipsoidal shape of arbitrary aspect ratio. They showed that the streamlines lie in a plane parallel to the shear plane and that when the vesicle shape departs markedly from the spherical shape the revolution velocity varies along the contour in a way that the velocities are smaller towards the poles of the vesicle. Very recent theoretical works dealt numerically with the full problem of the motion of vesicles, including the effects of thermal fluctuations, but they did not focus on surface flows.<sup>15</sup> Contrarily to the case of non-bounded shear flows, the surface flow of vesicles firmly adhered to a plane wall in a shear flow has not generated many experimental studies,<sup>9,16</sup> although the question is of interest in

<sup>a</sup>Laboratoire Adhésion et inflammation, Inserm U600/CNRS UMR 6212 Université de la Méditerranée, Case 937, 163 Avenue de Luminy, 13288 Marseille Cedex 09, France. E-mail: viallat@marseille.inserm.fr; Fax: 33 491 82 75 80; Tel: 33 491 82 75 77

<sup>b</sup>Laboratoire des Colloïdes, Verres et Nanomatériaux, Université Montpellier 2 & CNRS UMR 5587, Place Eugène Bataillon, 34095 Montpellier Cedex 05. E-mail: massiera@lcvn.univ-montp2.fr; Fax: 33 46714 46 37; Tel: 33 46714 39 82

terms of the mobility and recruitment of cell membranar receptors towards the adhesive zone on the substrate, which bear associated ligands.<sup>17</sup> Two theoretical works describe the motion of bound vesicles under flow,<sup>18,19</sup> focusing their studies on the unbinding of non-specifically adhered vesicles, but do not describe the membrane flow. The main questions we want to address in this paper are: is the vesicle membrane able to flow in the presence of attractive interaction with the substrate, either induced by the binding of specific membranar linkers or by a non-specific adhesive field? What are the characteristics of surface streamlines and the associated velocity field? How do these features vary with the vesicle size and the contact area?

The paper is organized as follows. After the description of materials and methods, we present the observation of vesicle shape and surface flows under shear flow. We characterize the streamlines on the vesicle surface as a function of the relative size of the contact zone with the substrate. Then, we determine the variation of the angular velocity along a streamline with its position on the surface. We finally briefly discuss the obtained results.

## Experimental

### Substrates

Two types of substrate were prepared in order to induce either non-specific adhesion (charged coverslips covered by poly-L-lysine) or specific adhesion (coverslips covered by histidine ligands). All products were purchased from Sigma except the histidine peptide (KGGSGSYGGSGGSHHHHH) obtained from Covalab (Villeurbanne, France). Adhesion was induced by chelation between two histidine groups and a nickel ion. The stability constant<sup>20</sup> of the complex  $C^*$ ,  $K = [C^*]/[Ni][Hist]^2$ , is equal to  $10^{15.9}$ .

Prior to any chemical treatment, glass coverslips were cleaned by immersion in a 14.5 M NaOH solution for 5 minutes and rinsed extensively with pure water. Polylysine coverslips were obtained by incubation in a polylysine solution ( $10^{-3}\%$  v/w) for 30 min, followed by rinsing with ultrapure water. The histidine functionalization was obtained according to the following process: a glutaraldehyde peptide was first bound to the silane activated glass surface by reaction between an aldehyde bond on the peptide and an amine bond on the silane. The histidine peptide was then bound to the glutaraldehyde peptide *via* its terminal amine function. The 6-histidine peptide was chosen since it maximizes the probability of chelation of Ni to a vesicle.<sup>21</sup> Technically, the glass slides sequentially received the following treatments at room temperature: incubation in a silane solution (1% v/v 3-aminopropyltriethoxysilane and 5 mM acetic acid in water) for 20 minutes under gentle mixing, rinsing with pure water, curing for 15 min at 100 °C and incubation in a glutaraldehyde solution (10% w/w) for 90 min under gentle mixing. The coverslips were then incubated for 2 hours at 37 °C in a solution of histidine peptide ( $1.2 \text{ mg ml}^{-1}$ ) diluted in a carbonate/bicarbonate buffer (0.2 M, pH = 8). After rinsing with a PBS–Triton solution (1%), the coverslips were incubated for 1 hour at 37 °C in an ethanolamine solution (0.2 M at pH = 10) in order to passivate the substrates and to prevent non-specific adhesion. The coverslips were rinsed

again using the PBS–Triton solution. Finally, the substrates were incubated in a sodium borohydride ( $\text{NaBH}_4$ ) solution ( $3.5 \text{ mg ml}^{-1}$ ) at room temperature for 1 hour without shaking, to reinforce the bond between the glutaraldehyde and the peptide (reduction of the the imine group of the glutaraldehyde/peptide bond into an amine group). The coverslips could then be stored for up to 8 days at 4 °C in a sodium azide–PBS buffer (0.1%  $\text{NaN}_3$  v/v).

### Vesicles

The lipids, 1,2-dioleoyl-sn-glycero-3-phosphocholine (DOPC) and 1,2-dioleoyl-sn-glycero-3-[[*N*-(5-amino-1-carboxypentyl)iminodiacetic acid]succinyl] (nickel salt) (DOGS-NTA-Ni) were purchased as a powder from Avanti Polar Lipids, and diluted at  $2 \text{ mg ml}^{-1}$  in a chloroform–methanol solution (9 : 1). Giant unilamellar lipid vesicles were prepared either from pure DOPC or from a 95 : 5 mixture of DOPC and DOGS-NTA-Ni, using the standard electroformation method.<sup>22</sup> Sucrose solutions (50 mM and 200 mM) were used as the internal fluid. The vesicles were then diluted in a solution of glucose with the same osmolarity as the internal solution of sucrose and were prepared in a HEPES buffer (10 mM, pH 8).

### Microscopy

‘Side view’ observation was obtained by orienting a phase contrast inverted microscope (Leica DM IRB, Wetzlar, Germany) horizontally and by working at low-angle incidence. The observation plane is then parallel to gravitational force and to the shear plane.<sup>8</sup> It provides well-defined side-view images of both vesicles and their reflections on the substrate. Most observations were performed with a phase contrast 20X objective (long working distance). Pictures were captured with a CCD (Cohu) and a dvcam video-recorder (Sony, DSR-25).

Reflection interference contrast microscopy (RICM) was used to determine the contact area of the adhered vesicle with the substrate.<sup>23</sup> This microinterferometric technique generates an intensity pattern by interference of two reflected rays: the incident light reflected both from the glass–buffer interface and from the buffer–vesicle interface. Strongly bound parts of the membrane appear as dark regions on the characteristic RICM patterns. Both standard “bottom view” observation and RICM observation were performed using a phase contrast inverted microscope (Olympus, IX71) equipped with an antireflective objective (Plan Neofluar,  $\times 63/1.25$  Oil, Zeiss). Epi-illumination through the objective was rendered monochromatic by passing light from a 100 W Hg vapor lamp (Olympus) through an interference filter (Ilg 546.1 nm).

### Flow

For side view observation, the flow chamber was a parallel piped-plate chamber (spectrophotometric circulation chamber from Hellma (Müllheim), height = 1 mm, width = 11.5 mm, length = 65 mm) with four optical faces. At one end, a rectangular opening gave us the possibility to introduce a coverslip. The laminar shear rate (from 1 to  $12 \text{ s}^{-1}$ ) was applied with a 20 mL syringe mounted on a syringe pump. Shear rate calibration was performed by measuring the

translational speed of polystyrene beads ( $2\ \mu\text{m}$  of diameter) vs. their distance from the substrate. For bottom view experiments, the chamber was a plexiglas block bearing a cavity of  $15.9 \times 9.9 \times 0.9\ \text{mm}^3$  surrounded by a toric gasket. Histidine or polylysine coverslips were maintained against the gasket with a screwed steel plate.

### Measurement protocol

Measurements were performed at a distance of less than  $50\ \mu\text{m}$  from the substrate, so that the shear rate can be taken as constant and equal to the wall shear rate. All vesicles studied were at a minimal distance of  $1\ \text{mm}$  from the nearest optical face of the chamber, so that velocity field and wall shear rate values were not disturbed by the presence of the side walls. Vesicles were slowly injected in the chamber and allowed to settle. One well-contrasted axisymmetric vesicle was chosen at rest. A flow was then applied. The wall shear rate applied to the vesicle was then increased gradually from  $1.3\ \text{s}^{-1}$  to  $11\ \text{s}^{-1}$ , by increasing the flow rate in the chamber step by step.

### Image analysis

For side view image analysis, we developed an IDL (RSI) code to determine the vesicle contour. Both the vesicle and its reflection were fitted by a sphere, and their intersection determined the adhesion parameter (contact length =  $L$ ). The membrane defect position was either tracked using an IDL tracking code,<sup>24</sup> or manually selected on each image using ImageJ software,<sup>25</sup> depending on the contrast.

## Results and discussion

We first determine the vesicle shapes. We then show the existence of surface flows in the part of the membrane, which is not in the close vicinity of the substrate. We then determine the surface streamlines and the angular velocity of the streamlines.

All coordinates are indicated by using a Cartesian referential:  $x$  = flow direction;  $y$  = shear direction.

### Determination of vesicle shapes

The projection of vesicles onto their meridian plane ( $z = 0$ ) is directly observed by side-view microscopic imaging (Fig. 1). Shapes are stable in time and do not significantly change upon increasing shear rate. They are well-described by truncated spheres, when the shear rate is less than  $12\ \text{s}^{-1}$ . It suggests that adhesion is strong, *i.e.*,  $WA \gg \kappa$ , where  $W$  is the adhesion energy per unit area,  $A$  the area of the adhesion disk and  $\kappa$  the bending rigidity of the membrane.<sup>26,27</sup> The shapes are characterized by their radius  $R$  and the position of the substrate ( $y = y_s$ ) relatively to the sphere centre, which is taken as the origin of the referential. One directly derives the diameter  $L$  of the contact zone in strong interaction with the substrate as shown in Fig. 1b. The full vesicle shape is determined by considering that the vesicles are axisymmetric about the  $y$ -axis.

The projection of vesicles onto their equatorial plane ( $y = 0$ ) is directly observed from regular “bottom view” phase contrast observation in the horizontal plane and yields vesicle radii (Fig. 2a). Moreover, simultaneous RISM observations

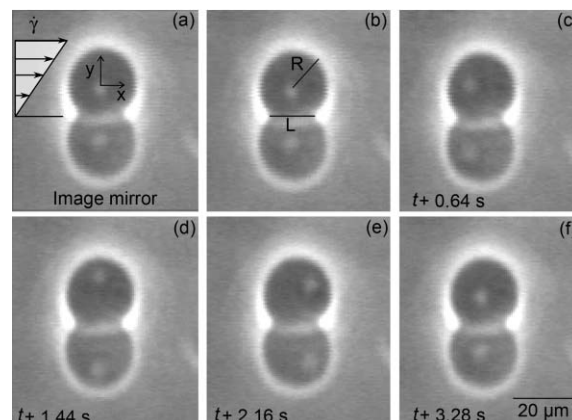


**Fig. 1** (a): Side view of a vesicle (Ves4) and its reflection on the substrate subjected to a linear shear flow along the  $x$  direction. (b):  $L$  is the length of the contact zone.  $R$  is the vesicle radius. From (b) to (f): we infer the surface flow from the motion of a lipid defect (clear dot), we used as a marker.

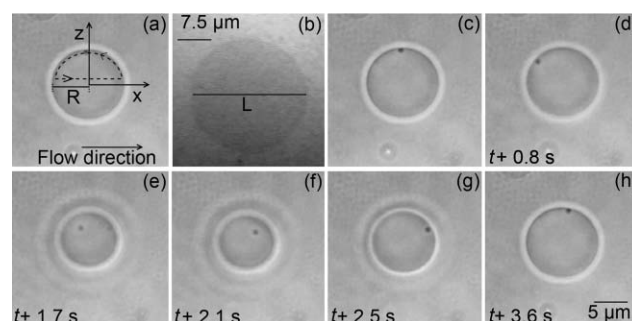


**Fig. 2** (a): Bottom view of Ves5, subjected to a linear shear flow. The dotted line represents the projection of the marker trajectory. (b): RISM view of Ves5 (the scale is different from (a), (c)–(h)). The adhesive zone corresponds to the large homogenous dark disc. (c), (d) and (h): the marker (black dot) avoids the contact zone when approaching the substrate. From (e) to (g) the marker circulates at the vesicle top (the focus varies).

show a strong interaction of the vesicle with the substrate over a large homogeneous disk of diameter  $L$  (Fig. 2b). There is no interference fringe at the edge of the contact zone due to a sharp slope of the membrane relative to the substrate. Observation in the horizontal ( $y = \text{constant}$ ) plane does not allow the full determination of the vesicle shape, since the vesicle axis of symmetry is perpendicular to the plane of observation. Based on side view observations, we assume that the shape of these vesicles is also a truncated sphere.

Geometrical characteristics of the vesicles studied are reported in Table 1. The vesicles exhibit large contact areas,  $L/2R$  values ranging from 0.46 to 1 (half-sphere). As all vesicles were suspended in a solution of the same osmolarity as that of the vesicle inner solution, they were expected to be swollen and present a spherical shape. We therefore assume that upon adhering to the substrate, the vesicles transiently opened several pores to release a part of the internal solution in order to relax the line tension on the membrane.<sup>28</sup> It should be emphasized that the shape of these adhering vesicles, which consists of a circular disk-like area on the substrate, a spherical



**Table 1** Experimental parameters for seven vesicles.  $L$  is the diameter of the contact area, and  $R$  the radius of the vesicles

Name	Radius/ $\mu\text{m}$	$L/2R$	Substrate
Ves1	11.0	0.46	Histidine
Ves2	11.0	0.89	Histidine
Ves3	17.5	0.90	Histidine
Ves4	10.9	0.74	Histidine
Ves5	18.4	0.96	Polylysine
Ves6	9.4	1.0	Polylysine
Ves7	11.4	0.98	Polylysine

cap on the opposite side, and a very small intermediate region of strong curvature along the contact line, reveals a large adhesion energy with the substrate.<sup>29</sup>

### Surface flow observation

We followed the movement of small defects (small clumps of lipids) bound to the vesicle membrane (approximate size 1  $\mu\text{m}$ ) under shear flow. We selected defects associated with the inner part of the membrane, which may theoretically circulate on the inner side of the membrane even if it is in the immediate vicinity of, or in contact with, the substrate.

The movement of these markers allows one to visualize the projection of surface motion. Sequences shown in Fig. 1 and Fig. 2 clearly demonstrate the existence of surface flows of the membrane, as already reported in refs 9 and 16. The projection of the orbits described by the defects on the surface are determined by measuring their position as a function of time as shown in Fig. 1 and are assumed to correspond to the surface streamlines on the membrane. It is worth emphasizing that the Brownian motion of a defect is slow compared to the velocity at which it circulates on the membrane and does not perturb the determination of the surface streamlines. On a longer timescale, however, the defects slowly diffuse on the membrane surface and explore various surface streamlines. The observation of the movement of a single defect, therefore, allows the determination of several orbits on a single vesicle.

The sequence in Fig. 2 shows that when the defect passes at the top of the vesicle membrane ( $x = 0$ ), its orbit is quasi-circular and lies in the plane ( $z = \text{constant}$ ) parallel to the shear plane. When it approaches the substrate, as detected by the change of focus of the defect, its trajectory departs from the plane and avoids the contact zone. This zone and the water molecules that can possibly lie between the vesicle and the substrate are therefore considered to be motionless.

### Streamline determination

The streamlines on each vesicle surface were obtained from the observation of a single defect. Its couple of coordinates ( $x, y$ ) and ( $x, z$ ) is directly measured from the side view (projection on the plane  $z = 0$ ) and regular bottom view (projection on the plane  $y = 0$ ) respectively. The third coordinate is calculated from the description of the vesicle as a truncated sphere of equation  $x^2 + y^2 + z^2 = R^2$  and  $y > y_s$ . The projections of streamlines are illustrated on three vesicles in three planes ( $x, z$ ), ( $x, y$ ) and ( $z, y$ ) in Fig. 3. Data are either obtained from direct observation or from determination of one coordinate *via* the sphere equation. The three vesicles exhibit various aspect

ratios, characterized by  $L/2R$ . Typical streamlines are illustrated in Fig. 3. The first feature to notice is that the surface flow is divided into two symmetric quadrants observed on each side of the meridian plane  $z = 0$ . The defect that moved in the meridian zone had changed side during the observation time, as illustrated in Fig. 3c. The second feature is that two stagnation points are observed on each side of the vesicle. As the vesicles are not spherical, the axis  $z$  is not a symmetry axis so that the stagnation points are not located on this axis, contrarily to what was observed for spherical vesicles sliding along an inclined plane.<sup>10</sup> The position of the stagnation point lies on the median plane  $x = 0$  and is located by the angle  $\theta$  between the radius of the sphere passing by this point and the axis  $z$  (Fig. 3). The variation of the angle  $\theta$  with the vesicle aspect ratio, characterized by the non-dimensional number  $L/2R$ , is reported in Fig. 4. The angle  $\theta$  starts from 0 for spherical symmetrical vesicles and slowly increases with  $L/2R$ . The increase is much sharper when  $L/2R$  approaches 1 (half-sphere). We did not observe vesicles with a ratio  $L/2R$  greater than 1 (with a contact angle greater than  $90^\circ$ ), which are likely to be very unstable due to the large bending energy of the membrane at the contact with the substrate.

When the size of the contact zone increases, the orbits of the streamlines depart more and more from planar circular orbits since no flow is allowed in the contact zone. The streamlines have non-trivial non-planar shapes, which are difficult to characterize (Fig. 3).

### Angular velocities

The period  $T$  of revolution of a defect on an orbit at the surface of a vesicle was experimentally determined by following the projection of marker trajectories over at least one full orbit. An example of the variation of the coordinates  $x$  and  $y$  of the marker *vs.* time, as deduced from side view imaging of the vesicle, is represented in Fig. 5. These variations are well fitted by a sinusoidal function, suggesting the rotational velocity is constant and equal to the frequency of revolution,  $\omega = 2\pi/T$ . Typical variation of  $\omega$  on one given orbit as a function of the shear rate  $\dot{\gamma}$  is illustrated in Fig. 6. The membrane velocity show several remarkable features. First, the velocity  $\omega$  varies linearly with the wall shear rate, as predicted for non-adhered vesicles in non-bounded shear flow<sup>14</sup> and observed on non-adhered vesicles flowing close to a substrate.<sup>8,11</sup> Moreover, for a given shear rate, the values of  $\omega$  increase upon decreasing the relative contact zone  $L/2R$ , *i.e.* upon modifying the aspect ratio of the vesicle. Finally, the rotational velocity on a given streamline depends on its lateral position on the vesicle surface. In order to illustrate this phenomenon, we measured the rotational velocity on various streamlines located on a single vesicle.

The lateral position of a streamline is characterized in the median plane of the vesicle ( $x = 0$ ) by the ratio  $s^* = s/s_0$ , of the curvilinear distance between the stagnation point and the streamline  $s$  to the curvilinear distance between the stagnation point and the vesicle top ( $x = 0, y = R, z = 0$ ),  $s_0$ , as shown in Fig. 3. Fig. 7 shows the variation of  $\omega/\dot{\gamma}$  with  $s^*$  for vesicles observed either from side or bottom view. Velocities are larger towards the stagnation points (SP). This variation is contrary

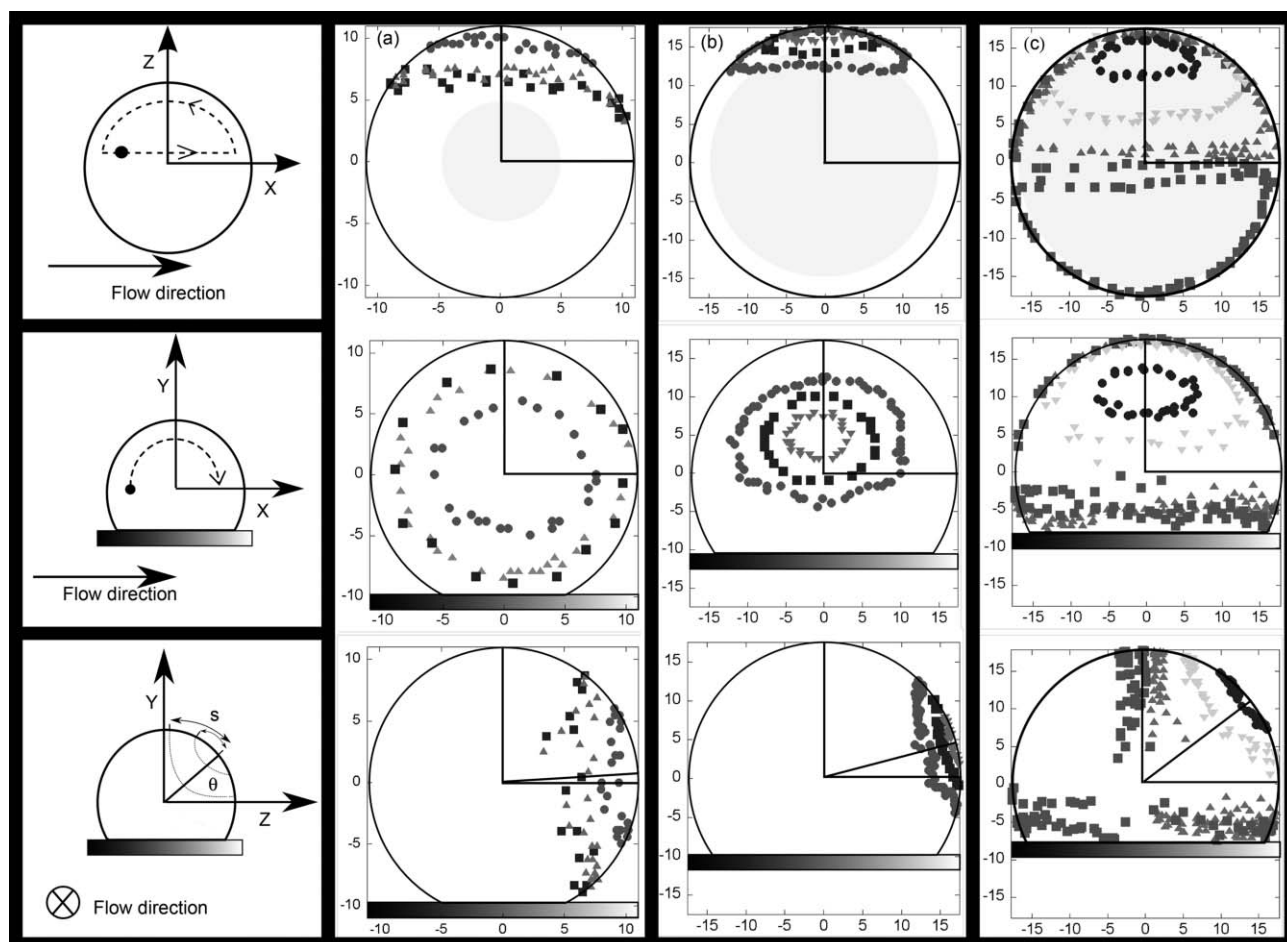


**Fig. 3** Marker trajectories and streamline reconstruction for three vesicles. Projection in the plane  $(x,y)$  of marker trajectories observed from side view imaging and reconstruction of the corresponding streamlines in  $(z,y)$  and  $(x,z)$  planes: (a): Ves1; (b): Ves3. Projection in the plane  $(x,z)$  of marker trajectories observed from bottom view imaging and reconstruction of the corresponding streamlines in  $(z,y)$  and  $(x,y)$  planes: (c): Ves5. The grey disc in the  $(x,z)$  view represents the contact zone.

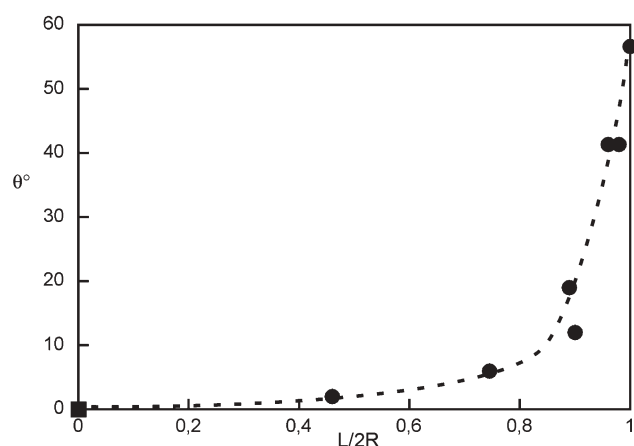


**Fig. 4** Variation of  $\theta$  (defined in Fig. 3) as a function of the aspect ratio  $L/2R$ . The dashed line is a guideline for the eyes.

to that predicted by Kraus *et al.*<sup>14</sup> on vesicles flowing in a non-bounded shear flow, where ellipsoid vesicles display smaller angular velocity towards the SP. Our result is likely to be due to the fact that the contact zone is motionless. It follows that

the angular velocities of the orbits at the proximity of the contact line must be small in order to limit the viscous dissipation in the membrane. The difference in angular velocity on the various streamlines reveals an effective strong shear in the membrane, since two adjacent lateral elements of the membrane do not remain adjacent after a full revolution. It is also noteworthy that the ratio  $\omega/\dot{\gamma}$  is greater than 0.5 close to the vesicle SP (also observed in ref. 11), this value being the angular velocity of a rigid fluid in a non-bounded shear flow.

We infer the two extreme values of the angular velocity,  $\omega_0$  at the vesicle top and  $\omega_\theta$  on the SP, by fitting the variation of the angular velocity with an arbitrary linear function,  $\omega/\dot{\gamma} = (\omega_0 - \omega_\theta)s^* + \omega_\theta$ , as displayed in Fig. 7. The quantity  $\omega_0 - \omega_\theta$  thus represents the gradient of velocity upon curvilinear displacement along the vesicle membrane. These three parameters are plotted vs. the aspect ratio,  $L/2R$ , in Fig. 8. It clearly appears that  $\omega/\dot{\gamma}$  is mainly determined by the vesicle aspect ratio  $L/2R$  and is weakly sensitive to the vesicle radius in the studied range.  $\omega/\dot{\gamma}$  is constant for  $L/2R \leq 0.8$ . For larger contact areas, the velocities sharply decrease and display a smaller difference between the top and the SP.

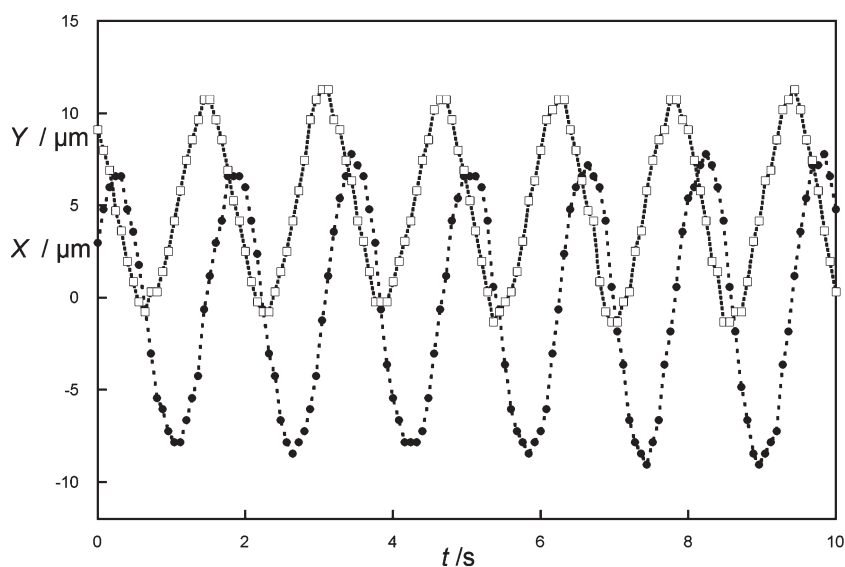


**Fig. 5** Typical time evolution of the coordinates  $x$  (black circles) and  $y$  (open squares) of a marker on Ves3 as deduced from side view imaging. The lines are guidelines for the eyes.

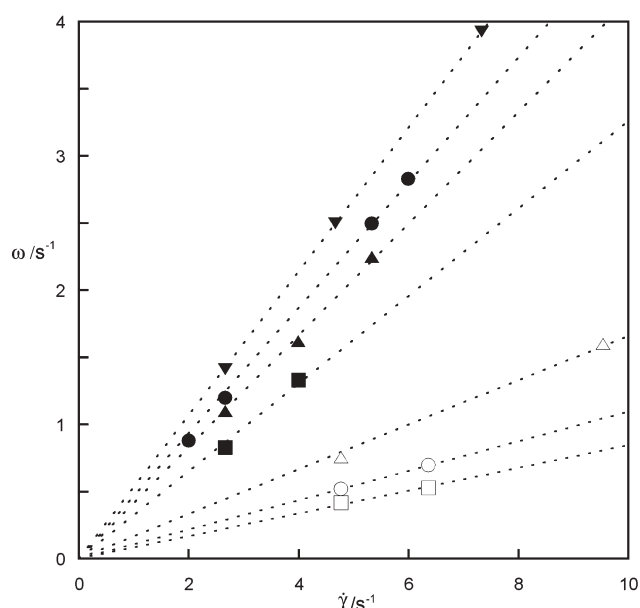


**Fig. 6** Linear variation of the angular velocity  $\omega$  of a circulating marker as a function of the shear rate  $\dot{\gamma}$  observed on fixed orbits: ●: Ves1; ■: Ves2; ▲: Ves3; ▼: Ves4; ○: Ves5; □: Ves6 and △: Ves7. Dashed lines are linear fit.

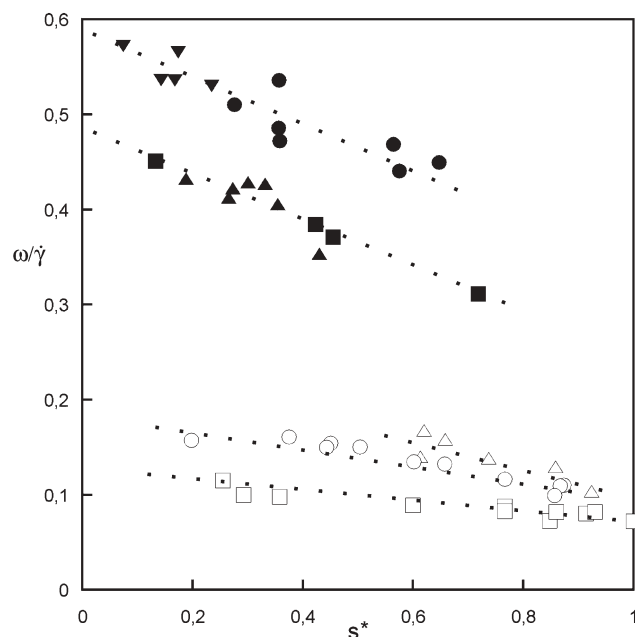


**Fig. 7** Variation of the reduced angular velocity  $\omega/\dot{\gamma}$  of a circulating marker as a function of the dimensionless curvilinear distance  $s^* = s/s_0$ . ●: Ves1; ■: Ves2; ▲: Ves3; ▼: Ves4; ○: Ves5; □: Ves6 and △: Ves7.  $\dot{\gamma}$  is varied in the range 1.13–11 s<sup>−1</sup>.

## Discussion

We described the main features of surface flows of giant lipid vesicles adhering to a substrate. We revealed the existence of fast flows on the surface associated with closed non-planar orbits around two stagnation points on each side of the vesicle. We showed that flow is very unlikely to occur in the adhesion zone with the substrate, meaning that the lipids do not bind and unbind at the rotational frequency of the membrane. It should be underlined here that the nature of the contact and thus the dissipation might be different for each kind of

adhesion: specific or non-specific. While non-specific adhesion will create a homogeneous contact area where all lipids are subjected to the interaction field with the substrate, specific adhesion implies domains of tight adhesion formed by Ni-lipids and histidine groups separated by non-adhesive or weakly adhesive areas containing pure DOPC lipids. These DOPC lipids may, in principle, flow around the bound lipids, though such a flow has a high cost in terms of energy of viscous dissipation.<sup>29</sup> The observation of local lipid flow requires more sophisticated instruments to be detected. The

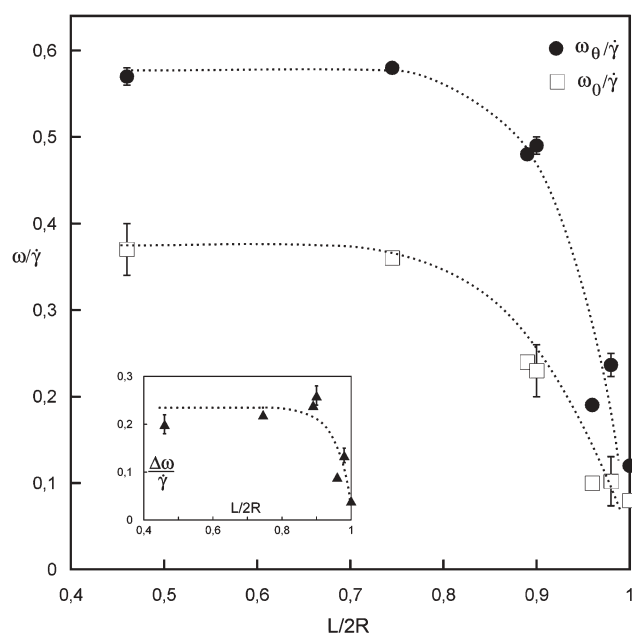


**Fig. 8** Variation of the reduced angular velocity extrapolated at the stagnation point,  $\omega_0/\dot{\gamma}$ , and at the vesicle top,  $\omega_\theta/\dot{\gamma}$ , vs. the aspect ratio  $L/2R$ . Insert: variation of the reduced gradient angular velocity as a function of  $L/2R$ . Dashed lines are guidelines for the eyes.

adhesive zone rather acts as an obstacle to the membrane flow, which therefore induces a velocity gradient. The angular velocity on the orbits indeed increases when the orbits are closer to the SP, showing a strong shearing dissipation in the membrane. However, as far as we know, no theoretical nor numerical description of the surface flows of the vesicle membrane is available today to describe the shape of the streamlines and the total viscous dissipation in the membrane. Similar questions have been addressed in the case of a drop adhered to a wall<sup>30,31</sup> but the streamlines are very different from the ones we observed since recirculation of surface molecules to the internal volume is authorized for drops, whereas lipid molecules cannot enter the inner vesicle volume, or in other terms, the surface divergence of the surface velocity must equal zero in the case of a lipid vesicle. In the case of a cell, a solid cytoskeleton is bound to the membrane via transmembranar proteins. As the contact zone is fixed and the cytoskeleton is an elastic solid, the whole cytoskeleton is expected to remain fixed over the whole cell. Therefore, no fast flow of the cell membrane is expected. Indeed, side view imaging revealed that small heterogeneities on CHO cells adhered to a glass substrate under shear flow are motionless.<sup>32</sup> However, a small lipid flow may occur around the transmembranar proteins, associated with a strong viscous dissipation as observed when a thread is pulled out from a cell.<sup>33</sup> The decrease in  $\omega/\dot{\gamma}$  with the adhesion strength, characterised by the ratio  $L/2R$ , could have multiple origins including: i) the fact that the larger the adhesive zone, the more the membrane flow is hindered by this obstacle, ii) Deviation from the spherical shape has previously been shown to decrease the ratio  $\omega/\dot{\gamma}$  as derived from theories describing the dynamics of a vesicle under shear flow.<sup>12–14</sup>

## Conclusion

We used a simple experimental approach to describe the fast surface flows of the lipid membrane of an adhered giant vesicle, which had not yet been studied. Our approach relied on the motion of markers, whose size is of the order of one micron.

It is worth underlining that molecular flow may also occur in the contact area, which might allow the recruitment of surface receptors towards the membrane adhesion zone. Other experimental tools, such as adapted fluorescence techniques (FRAP, FCS), could be of interest to give a further insight into the molecular flows on adhered cells and vesicles. Moreover, we hope that our work will generate numerical studies in order to better understand the dependence of the streamline shapes and of the membrane viscous dissipation as a function of the radius and of the aspect ratio of the vesicles.

We acknowledge Professor F. Bruckert for the design of the peptide and help in the functionalization process, Dr L. Limozin for RIMC experiments, Professor P. Bongrand for tracking numerical codes and Dr M. Abkarian for discussions. Parts of the experiments were performed in the Laboratoire de Spectrométrie Physique, UMR5588-University J. Fourier, Grenoble, France.

## References

- 1 H. Stone, A. Stroock and A. Ajdari, *Annu. Rev. Fluid Mech.*, 2004, **36**, 381.
- 2 R. Alon, D. A. Hammer and T. A. Springer, *Nature*, 1995, **374**, 539; K.-C. Chang, D. F. Tees and D. A. Hammer, *Proc. Natl. Acad. Sci. U. S. A.*, 2000, **97**, 11262.
- 3 H. Goldsmith and J. Marlow, *Proc. R. Soc. London, Ser. B*, 1972, **182**, 351.
- 4 T. Fischer and H. Schmid-Schnbein, *Blood Cells*, 1977, **3**, 351; T. Fischer, M. Stöhr-Liesen and H. Schmid-Schönbein, *Science*, 1978, **202**, 894.
- 5 C. E. Chaffey, H. Brenner and S. G. Mason, *Rheol. Acta*, 1965, **4**, 64.
- 6 H. Schmid-Schnbein and R. Wells, *Science*, 1969, **165**, 288.
- 7 K. H. de Haas, C. Blom, D. van den Ende, M. G. H. Duits and J. Mellema, *Phys. Rev. E: Stat., Nonlinear, Soft Matter Phys.*, 1997, **56**, 7132–7137.
- 8 M. Abkarian and A. Viallat, *Biophys. J.*, 2005, **89**, 1055; M. Abkarian, C. Lartigue and A. Viallat, *Phys. Rev. Lett.*, 2002, **88**, 8103–8107.
- 9 B. Lorz, R. Simson, J. Nardi and E. Sackmann, *Europhys. Lett.*, 2000, **51**, 468–474.
- 10 M. Abkarian, C. Lartigue and A. Viallat, *Phys. Rev. E: Stat., Nonlinear, Soft Matter Phys.*, 2001, **63**, 1–7.
- 11 A. Razpet, G. Gomisecek, V. Arrigler, S. Svetina and B. Zeks, *Eur. J. Physiol.*, 2000, **439** (suppl.), R141–R142.
- 12 S. Keller and R. Skalak, *J. Fluid Mech.*, 1982, **120**, 27–47.
- 13 T. W. Secomb and R. Skalak, *Q. J. Mech. Appl. Math.*, 1982, **XXXV**, 2, 233.
- 14 M. Kraus, W. Wintz, U. Seifert and R. Lipowsky, *Phys. Rev. Lett.*, 1996, **77**, 3685.
- 15 H. Noguchi and G. Gompper, *Phys. Rev. Lett.*, 2004, **93**, 8102.
- 16 D. Cuvelier, C. Vézé, A. Viallat, P. Bassereau and P. Nassoy, *J. Phys.: Condens. Matter*, 2004, **16**, S2427–S2437.
- 17 F. Brochard-Wyart and P. G. de Gennes, *Proc. Natl. Acad. Sci. U. S. A.*, 2002, **99**, 7854–7859.
- 18 S. Sukumaran and U. Seifert, *Phys. Rev. E: Stat., Nonlinear, Soft Matter Phys.*, 2001, **64**, 1–11; U. Seifert, *Phys. Rev. Lett.*, 1999, **83**, 876–879.
- 19 I. Cantat and C. Misbah, *Phys. Rev. Lett.*, **83**, 880–884.
- 20 R. M. C. Dawson, D. C. Elliott, W. H. Elliott and K. M. Jones, in *Data for Biochemical Research*, Oxford University Press, USA, 3rd edn, 1986, pp. 409.



- 21 M. Conti, G. Falini and B. Samori, *Angew. Chem., Int. Ed.*, 2000, **39**, 215–218.
- 22 M. I. Angelova, S. Soléau, P. Méléard, J. F. Faucon and P. Bothorel, *Prog. Colloid Polym. Sci.*, 1992, **89**, 127–131.
- 23 E. Sackmann and R. F. Bruinsma, *ChemPhysChem*, 2002, **3**, 262–269.
- 24 J. C. Crocker and D. G. Grier, *J. Colloid Interface Sci.*, 1996, **179**, 298–310; <http://www.physics.emory.edu/~weeks/idl/>.
- 25 ImageJ software: <http://rsb.info.nih.gov/ij/>.
- 26 U. Seifert and R. Lipowsky, *Phys. Rev. A: At., Mol., Opt. Phys.*, 1990, **42**, 4768; R. Lipowsky and U. Seifert, *Langmuir*, 1991, **7**, 1867.
- 27 C. Tordeux, J.-B. Fournier and P. Galatola, *Phys. Rev. E: Stat., Nonlinear, Soft Matter Phys.*, 2002, **65**, 041912.
- 28 R. Lipowsky and U. Seifert, *Mol. Cryst. Liq. Cryst.*, 1991, **202**, 17–25.
- 29 O. Sandre, L. Moreaux and F. Brochard-Wyart, *Proc. Natl. Acad. Sci. U. S. A.*, 1999, **96**(19), 10591–10596.
- 30 C. Pozrikidis, personal communication.
- 31 P. Dimitrakopoulos and J. J. L. Higdon, *J. Fluid Mech.*, 1997, **336**, 351–378.
- 32 A. Viallat, M. Faivre, M. Abkarian, C. Vézzy and N. Glade, presented in part at the Gordon Research Conference: colloidal, macromolecular and polyelectrolyte solutions, Ventura, USA, February, 2004.
- 33 F. Brochard-Wyart, N. Borghi, D. Cuvelier and P. Nassoy, *Proc. Natl. Acad. Sci. U. S. A.*, 2006, **103**, 7660–7663.

# Find a SOLUTION

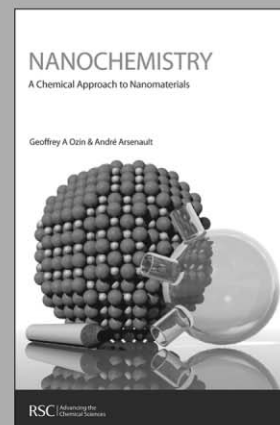
## ... with books from the RSC

**Choose from exciting textbooks, research level books or reference books in a wide range of subject areas, including:**

- Biological science
- Food and nutrition
- Materials and nanoscience
- Analytical and environmental sciences
- Organic, inorganic and physical chemistry

**Look out for 3 new series coming soon ...**

- RSC Nanoscience & Nanotechnology Series
- Issues in Toxicology
- RSC Biomolecular Sciences Series



**RSC** | Advancing the  
Chemical Sciences

[www.rsc.org/books](http://www.rsc.org/books)

28040542